Neurobiology of Disease 124 (2019) 479–488

Contents lists available at ScienceDirect

Neurobiology of Disease

journal homepage: www.elsevier.com/locate/ynbdi

Brain proteome changes in female *Brd1*$^{+/-}$ mice unmask dendritic spine pathology and show enrichment for schizophrenia risk

Veerle Paternoster[a,b,c,d,*], Maria Svanborg[a,b,c], Anders Valdemar Edhager[e], Anto P. Rajkumar[a,b,c,f,g], Esben Ahlburg Eickhardt[a,b,c], Jonatan Pallesen[a,b,c], Jakob Grove[a,b,c,h], Per Qvist[a,b,c], Tue Fryland[a,b,c], Gregers Wegener[d], Jens Randel Nyengaard[i], Ole Mors[a,b,d], Johan Palmfeldt[e], Anders Dupont Børglum[a,b,c], Jane Hvarregaard Christensen[a,b,c]

[a] The Lundbeck Foundation Initiative for Integrative Psychiatric Research, iPSYCH, Aarhus, Denmark
[b] Centre for Integrative Sequencing, iSEQ, Aarhus University, Aarhus, Denmark
[c] Department of Biomedicine, Aarhus University, Aarhus, Denmark
[d] Department of Clinical Medicine, Translational Neuropsychiatry Unit, Aarhus University, Aarhus, Denmark
[e] Research Unit for Molecular Medicine, Aarhus University Hospital, Aarhus, Denmark
[f] Mental Health of Older Adults and Dementia Clinical Academic Group, South London and Maudsley NHS Foundation Trust, London, UK
[g] Department of Old Age Psychiatry, Psychology, & Neuroscience, King's College London, Institute of Psychiatry, London, UK
[h] Bioinformatics Research Centre, BiRC, Aarhus University, Aarhus, Denmark
[i] Stereology and Electron Microscopy Laboratory, Centre for Stochastic Geometry and Advanced Bioimaging, Aarhus University Hospital, Aarhus, Denmark

ARTICLE INFO

Keywords:
Dendritic spine
Cytoskeleton
Proteomics
TMT10plex
Bromodomain containing 1
Animal model
Schizophrenia
Mitochondria

ABSTRACT

Genetic and molecular studies have implicated the Bromodomain containing 1 (*BRD1*) gene in the pathogenesis of schizophrenia and bipolar disorder. Accordingly, mice heterozygous for a targeted deletion of *Brd1* (*Brd1*$^{+/-}$ mice) show behavioral phenotypes with broad translational relevance to psychiatric disorders. *BRD1* encodes a scaffold protein that affects the expression of many genes through modulation of histone acetylation. BRD1 target genes have been identified in cell lines; however the impact of reduced *Brd1* levels on the brain proteome is largely unknown. In this study, we applied label-based quantitative mass spectrometry to profile the frontal cortex, hippocampus and striatum proteome and synaptosomal proteome of female *Brd1*$^{+/-}$ mice. We successfully quantified between 1537 and 2196 proteins and show widespread changes in protein abundancies and compartmentalization. By integrative analysis of human genetic data, we find that the differentially abundant proteins in frontal cortex and hippocampus are enriched for schizophrenia risk further linking the actions of BRD1 to psychiatric disorders. Affected proteins were further enriched for proteins involved in processes known to influence neuronal and dendritic spine morphology e.g. regulation of cytoskeleton dynamics and mitochondrial function. Directly prompted in these findings, we investigated dendritic spine morphology of pyramidal neurons in anterior cingulate cortex and found them significantly altered, including reduced size of small dendritic spines and decreased number of the mature mushroom type. Collectively, our study describes known as well as new mechanisms related to BRD1 dysfunction and its role in psychiatric disorders, and provides evidence for the molecular and cellular dysfunctions underlying altered neurosignalling and cognition in *Brd1*$^{+/-}$ mice.

1. Introduction

Repeated evidence from large genetic studies have implied that the bromodomain containing 1 (*BRD1*) gene has a role in susceptibility to schizophrenia (SZ) and possibly also to bipolar disorder (BD) (Nyegaard et al., 2010; Severinsen et al., 2006; K a et al., 2013; Purcell et al., 2014; Jorgensen et al., 2002; Andreassen et al., 2014; Pardiñas et al., 2016; Ripke et al., 2014). The SZ risk allele of the *BRD1* promoter SNP

Abbreviations: BD, bipolar disorder; BH, Benjamini-Hochberg; DAP, differentially abundant protein; DCP, differentially compartmentalized protein; FDR, false-discovery rate; LD, linkage disequilibrium; LFC, log2 fold change; GWAS, genome-wide association study; IAA, 2-Iodoacetamide; MS, mass spectrometry; SZ, schizophrenia; TCEP, tris(2-carboxyethyl)phosphine; FrC, frontal cortex; HC, hippocampus; ST, striatum; WT, wild type; Cell, cell lysate; Syn, synaptosome; LTP, long term potentiation; LTD, long term depression

* Corresponding author at: Department of Biomedicine, Wilhelm Meyers Allé 4, Building 1242, Room 235, 8000 Aarhus C, Denmark.
E-mail address: veerle@biomed.au.dk (V. Paternoster).

https://doi.org/10.1016/j.nbd.2018.12.011
Received 25 April 2018; Received in revised form 23 November 2018; Accepted 18 December 2018
Available online 24 December 2018
0969-9961/

rs138880 and SNPs in high linkage disequilibrium (LD) have been shown to be correlated with reduced *BRD1* mRNA expression (Qvist et al., 2016) as well as increased DNA methylation of the *BRD1* promoter (Dyrvig et al., 2017), suggesting that reduced *BRD1* expression might contribute to increase SZ risk. This is further indicated, by the identification of a SZ case with a disruptive nonsense mutation in *BRD1* (Purcell et al., 2014), even though *BRD1* is otherwise highly intolerant to loss of function mutations (Lek et al., 2016). BRD1, which is a scaffold protein that interacts with histone modifiers and chromatin remodelling proteins (Fryland et al., 2016; Mishima et al., 2011), seems to be functionally interconnected with a large number of schizophrenia risk genes by means of direct protein-protein interactions (Fryland et al., 2016) as well as by its genomic binding sites (Fryland et al., 2016) and gene regulatory effects (Qvist et al., 2016; Fryland et al., 2016; Rajkumar et al., 2018). The expression of *BRD1* itself is highly regulated during brain development (Severinsen et al., 2006) and stem cell differentiation (Cho et al., 2016) as well as by environmental stimuli like chronic restraint stress (Christensen et al., 2012), electroconvulsive seizures (Fryland et al., 2012) and commonly used mood stabilizers (Dyrvig et al., 2017). Underlining the impact of BRD1 on mental health, mice with a monoallelic inactivation of *Brd1* (*Brd1*$^{+/-}$ mice) are characterized by behavioral-, neuromorphological and neurochemical changes with broad translational relevance to psychiatric disorders (Qvist et al., 2016; Rajkumar et al., 2018; Qvist et al., 2017; Qvist et al., 2018). In female *Brd1*$^{+/-}$ mice, this includes reduced cortical serotonin, despair-like behaviors, impaired pre-attentive processing and neurocognitive deficits accompanied by aberrant morphology of pyramidal neurons and reduced dendritic spine density in anterior cingulate cortex (aCC) (Rajkumar et al., 2018; Qvist et al., 2017). Furthermore, genomic and transcriptomic studies have revealed that BRD1 might act as a modulator of nuclear receptor mediated signaling, which may explain sex-biased symptom profiles (Fryland et al., 2016; Rajkumar et al., 2018). Although, expression profiles have been generated by RNAseq for selected brain regions to characterize molecular signatures in *Brd1*$^{+/-}$ mice (Qvist et al., 2016; Rajkumar et al., 2018), the effects of BRD1 deficiency on protein abundancies in the brain remains largely unknown. Here, we thus investigated the brain proteome in *Brd1*$^{+/-}$ mice using quantitative mass spectrometry (MS) and labelling with isobaric tags (Tandem Mass Tags, TMT). We set out to map the proteome composition of three different brain regions: frontal cortex (FrC), hippocampus (HC) and striatum (ST), and additionally applied synaptosomal proteomics of the same tissues to further decipher differences in protein abundancy and cellular compartmentalization caused by BRD1 deficiency in the brain. Our findings are followed up by integrative analyses using human genetic data and detailed analysis of dendritic spine morphology in mice.

2. Materials and methods

2.1. Animals

Brd1$^{+/-}$ mice are heterozygous for an inactivated allele of *Brd1* (Qvist et al., 2016). Female *Brd1*$^{+/-}$ and wild type (WT) littermates were sacrificed at age 6–8 weeks by cervical dislocation and brain tissues (frontal cortex, hippocampus and striatum) were collected by free-hand dissection, snap frozen and stored at −80 °C upon further use (**Suppl. Information 1**). All studies were carried out in accordance with Danish legislation, granted by the animal welfare committee, appointed by the Danish Ministry of Food, Agriculture and Fisheries – Danish Veterinary and Food Administration.

2.2. Protein isolation

Brain regions were homogenized using pestles from the Grinding Kit (GE Healthcare, Chicago, Illinois, USA) in core buffer as previously described (Chang et al., 2012) supplemented with 1 Complete Mini Protease Inhibitor Cocktail tablet (Roche, Penzberg, Germany) per 10 ml buffer. The homogenate was split in two fractions for total cell lysate and for enrichment of synaptosomes, respectively. The total cell lysate was prepared by two repeated freeze-thaw cycles, bath sonication and centrifugation at 12000 rpm for 5 min. The supernatant was isolated and stored at −20 °C upon further use. The synaptosomal fraction was prepared as described before with minor adaptations (Chang et al., 2012). In short, the homogenate was filtered through a 5 μm membrane (Millipore, Billerica, Massachusetts, USA). Thereafter the flow-through was centrifuged to pellet the synaptosomal fraction. The frontal cortex samples for MS analysis were redissolved in core buffer. The frontal cortex (for validation), hippocampal and striatal samples were redissolved in 0.1% SDS in core buffer and sonicated at maximum intensity for 1 min. Total protein concentration of all fractions was measured with the Fluoroprofile Protein Quantification Kit (Sigma Aldrich, St. Louis, Missouri, USA) according to manufacturer's recommendations.

2.3. Western blotting analysis

Protein samples were diluted to 2.5 mg/ml in reducing loading buffer (Life Technologies, Waltham, Massachusetts, USA), boiled at 95 °C for 10 min and loaded on a Criterion™ TGX Stain-Free™ SDS PAGE gel (Biorad, Hercules, California, USA). After size separation, the gel was activated for 4 min under UV light. The proteins were then transferred to a low fluorescence PVDF membrane (Biorad). The membrane was blocked in 10% skimmed milk buffer (Millipore) and incubated with one of the following primary and appropriate secondary antibodies: anti-beta actin (Abcam, Cambridge, United Kingdom, #ab6276, 1:25000), anti-PSD95 (Millipore #MAB1596, 1:700), anti-VDAC1 (Abcam #ab15895, 1:25000), anti-GAP43 (Santa Cruz, Dallas, Texas, USA #SC10786, 1:1000), anti-HSP60 (Sigma Aldrich, #H3524, 1:25000), anti-NDUFA9 (Mitoscience, Eugene, Oregon, USA, #MS111, 1:25000), anti-NF200 (Sigma Aldrich, #N4142, 1:1000), anti-GFAP (Sigma Aldrich, #G3893, 1:10000), goat anti-rabbit antibody (Dako, Glostrup, Denmark, #P0448), and goat anti-mouse antibody (Dako, #P0447). The membrane was developed with Pierce ECL Plus Western Blotting Substrate (Thermo Scientific, Waltham, Massachusetts, USA) and visualized with Image Quant LAS-4000 Imager (GE Healthcare). Antibody sensitivity was tested for by checking for linear response to increased protein amounts (standard curve from a pool of all samples, four points between 12.5 and 50 μg total protein loaded). Protein abundances of samples within an extrapolated range of the standard curve (± 7 μg of the most extreme points from the standard curve) were calculated based on the standard curve and normalized to total protein intensity of transferred proteins (minimum 3 samples per group).

2.4. Sample preparation for mass spectrometry

Protein samples were prepared for labelling by TMT10plex Mass Tag Labelling (Thermo Scientific) according to the manufacturer's protocol. In short, 100 μg of total protein was reduced and alkylated with tris(2-carboxyethyl)phosphine (TCEP) and 2-Iodoacetamide (IAA), followed by overnight acetone precipitation. After redissolving the pellet, proteins were digested overnight with trypsin (Promega, Fitchburg, Wisconsin, USA). Resulting peptides were labelled with the TMT10plex Mass tags and the 10 samples were pooled. Labelled peptide pools were dissolved in 0.1% formic acid p*H* 2.3, before being fractioned into 8 fractions using Oasis MCX μElution (Waters Corporation, Milford, Connecticut, USA). Peptides were stepwise eluted in seven 50 mM ammonium formate buffers, containing 15% (first eluate) or 35% (all other eluates) methanol and with acidity ranging between p*H* 2.6 and p*H* 9. The final fraction was eluted with a buffer containing 35% methanol and 5% NH_4OH.

2.5. NanoLC-MS/MS

Liquid chromatography tandem mass spectrometry (LC-MS/MS) was performed on an EASY nanoLC-1000 coupled to Q Exactive™ Plus Hybrid Quadrupole-Orbitrap™ Mass Spectrometer (Thermo Scientific). TMT tagged peptide samples were trapped on a pre-column (PepMap 100, C18, 2 cm, 75 µm i.d., 3 µm, 100 Å, Thermo Scientific) followed by separation on a C18 reverse phase column with integrated emitter (EASY-Spray column, Plug and spray, PepMap 25 cm, 75 µm i.d., 2 µm, 100 Å, Thermo Scientific). Separation was conducted using Buffer B containing 90/10 acetonitrile/water and 0.1% formic acid at a flowrate of 300 nL/min in a 90 min linear gradient (4 to 40% Buffer B). The MS was operated in a positive data dependent mode, automatically switching between MS1 (full scan) and MS2 (fragmentation scan) acquisition. Resolution of MS1 was set to 70,000 and MS2 to at least 35,000. In MS1, AGC target was set to 1×10^6 ions and scan range between 380 and 1800 *m/z*. In MS2, AGC target was set at 2×10^5 ions, with fixed first mass set to 120 m/z. Dynamic exclusion was set to 20 s, isolation window at 2.0 m/z, and up to ten of the most intense ions were fragmented after every MS1 scan, by higher-energy C-trap dissociation (HCD). Ions with single charge or unassigned charge states were excluded from fragmentation.

LC-MS/MS analyses were performed three times for each peptide sample, with the third analysis applying an exclusion list of the 100 most intense peptide peaks. All three LC-MS analyses of the same sample set were merged and submitted to database searches for protein identification and quantification.

2.6. Data analysis

Peptide identification was performed in Proteome Discoverer 1.4 (Thermo Scientific) using the Mascot (Matrix Science, Boston, Massachusetts, USA) database algorithm and the Percolator algorithm (Brosch et al., 2009), with UniProt Knowledgebase release 2014_10 (Number of sequences after taxonomy (*Mus musculus*): 16693) as reference proteome. The following settings were applied: total intensity threshold of 20,000; precursor mass tolerance of 7 ppm; fragment mass tolerance of 10 mmu; peak integration tolerance of 10 ppm; minimum MS/MS peak count of 20; maximum 2 missed trypsin cleavages allowed. Only protein-unique peptides with FDR < 0.01 and co-isolation < 40% were included in the analysis. Proteins with at least 2 unique peptides and minimum 3 scans were considered for quantification. Raw peptide intensities were normalized using LOESS regression (0.4 window width) in the InfernoRDN software (Polpitiya et al., 2008). Protein abundances were then obtained by the RRollup algorithm (Polpitiya et al., 2008). Differentially abundant proteins (DAPs) were identified by PLGEM (Pavelka et al., 2008; Pavelka et al., 2004). Log2 fold change (LFC) cut-off was set as two times the global standard error of the mean of the dataset. Proteins were considered differential abundant between *Brd1*$^{+/-}$ and WT mice if both $p < .05$ and LFC > cut-off value. Proteins were considered as 'top DAPs' when $p < .001$ and LFC > cut-off. To identify differentially compartmentalized proteins (DCPs), the synaptosome-to-cell lysate abundancy ratio was calculated for all proteins detected in both datasets from the same brain region. Ratios were compared between genotypes using PLGEM. Proteins are considered DCPs when $p < .05$.

Mitochondrial proteins were selected according to Pagliarini et al. with a cut-off threshold corrected false discovery rate (cFDR) set at 7% according to previously reported research (Pagliarini et al., 2008) and to MitoMiner with positive score in at least 4 of the evidence lines (Smith et al., 2012). Mouse protein IDs were converted to the human homolog Ensembl Gene ID for bioinformatic analysis using the db2db online tool (Mudunuri et al., 2009). DAVID bioinformatics tools were used for Functional Annotation Clustering (Huang et al., 2009) with standard settings and using all identified proteins of the specific brain region as background. Protein-protein interaction network analysis was performed using the STRING database employing standard settings (Szklarczyk et al., 2015). Enrichment analysis for transcription factor binding was performed using Enrich (Chen et al., 2013) (ENCODE and ChEA Consensus TFs from ChIP-X) using default settings. Risk gene enrichment analysis was performed using MAGMA (de Leeuw et al., 2015) with default settings and using all identified proteins of the specific brain region as background. The analysis was based in summary statistics from single-marker genome-wide association studies (GWASs) (Ripke et al., 2014; Lambert et al., 2013; Major Depressive Disorder Working Group of the Psychiatric GWAS Consortium, 2013; Cross-Disorder, 2013; Psychiatric GWAS Consortium Bipolar Disorder Working Group, 2011; Wood et al., 2014; Demontis et al., 2019; Grove et al., 2017) (excluding the broad MHC region (chr6: 25 M–35 M)) and filtered for info score ≥ 0.8 if available. Genes were annotated using Ensemble (GRCh38.p12). Information about linkage disequilibrium was obtained using the 1000 Genomes European panel (Genomes Project Consortium, 2012).

2.7. Availability of data

The mass spectrometry proteomics data have been deposited to the ProteomeXchange Consortium via the PRIDE partner repository with the dataset identifier PXD009688; PXD009689; PXD009690; PXD009691; PXD009692; PXD009961.

2.8. Dendritic spine morphology

Dendritic spine morphology analysis was performed using the Golgi-cox stained brain slices derived from an independent set of mice and 3D reconstructed pyramidal neurons described previously (**Suppl. Information 1**) (Rajkumar et al., 2018). Identification and analysis of dendritic spines was done with IMARIS 7.7.1 software. Classification of spine types was done with following settings: Stubby (length < 1 µm), Mushroom (length < 3 µm and max diameter (head) > 2× mean width (neck)), Long Thin (mean width (head) ≥ mean width (neck)), and Filopodia / Dendrite (rest).

Continuous parameters were analyzed using a linear mixed-effects model (lmer function in the R package lme4 (Kuznetsova et al., 2016)), binary parameters were analyzed using a generalized linear mixed-effects model (glmer function in the R package lme4 (Kuznetsova et al., 2016)) as previously described (Paternoster et al., 2017). All models included spine level and depth (as defined by IMARIS) and genotype as explanatory variables, and neuron and mouse as level identifiers. Significance testing of contribution of parameters was conducted using the lmerTest package in R (Kuznetsova et al., 2016) and BH correction was applied to correct for multiple testing.

3. Results

3.1. BRD1 deficiency is associated with widespread changes in protein abundancies in brain

To discover novel BRD1 dependent molecular changes in the brain, we profiled differentially abundant proteins (DAPs) in three brain regions which show differential neurochemistry and mRNA expression levels and which are involved in observed behavioral changes in female *Brd1*$^{+/-}$ mice (Rajkumar et al., 2018; Qvist et al., 2017): frontal cortex (FrC), hippocampus (HC) and striatum (ST). By subjecting total cell lysates (Cell) and extracts enriched for synaptosomes (Syn) to MS-based quantitative proteomics using TMT10plex (Fig. 1) we obtained six protein datasets (FrC-cell, FrC-syn, HC-cell, HC-syn, ST-cell, and ST-syn) (**Suppl. Information 2,**Suppl. Fig. 2). All datasets were checked for gross differences in cell composition using cell type specific markers and one sample from FrC-Syn was removed from further analysis due to an apparent diverging proportion of oligodendrocytes (**Suppl. Information 2,**Suppl. Fig. 2). We observed a shift in the mitochondrial

subproteome (69/234 (29%) detected mitochondrial proteins are identified as DAPs, of which 66 are downregulated in *Brd1*$^{+/-}$ mice compared to WT) in the FrC-syn dataset, which was subsequently removed to avoid bias in normalization (**Suppl. Information 3,**Suppl. Fig. 4). Overall, we detected 1880 unique proteins in FrC (both datasets combined), 2370 unique proteins in HC (both datasets combined) and 1978 unique proteins in ST (both datasets combined) (Suppl. Table 2). Because no protein remained significant after BH-correction for multiple testing in any of the datasets, we classified 16 proteins as 'top DAPs' (Fig. 2 and Table 1). These top DAPs could be categorized in six groups based on function (Fig. 2 and Table 1): Transcription & chromatin (6 top DAPs), neuronal morphology and growth (4 top DAPs), cellular transport (2 top DAPs), neuroendocrine (2 top DAPs), and other (2 top DAPs). We selected 4 proteins from frontal cortex for validation by Western blotting analysis in an independent set of samples: 3 mitochondrial proteins (VDAC1, HSP60 and NDUFA9) and GAP43. After exclusion of HSP60 for technical reasons, we were able to confirm the differential abundancies of 2 out of the 3 remaining proteins (NDUFA9 and GAP43) (**Suppl. Information 4).** Additionally, we found significantly less PSD95 in *Brd1*$^{+/-}$ mice in FrC-syn (LFC = −0.10, p = .0480). This is in line with previously observed reduced dendritic spine density in anterior cingulate cortex (aCC), (Rajkumar et al., 2018) thereby further validating our findings.

3.2. DAPs are interconnected and cluster in functions related to mitochondria and the cytoskeleton

To inform about a potential biological role of the DAPs, we first performed a protein-protein interaction (PPI) enrichment score analysis using the STRING algorithm (**Suppl. Information 5**). DAPs in all brain regions, except HC-cell were significantly enriched for PPIs, with enrichment ratios ranging from 3.31 (FrC-cell) to 26.14 (ST-cell), meaning that DAPs within these datasets are at least partly biologically interconnected. The lack of significant results among DAPs from HC-cell is likely due to the lack of power as a result of the low number of DAPs (n = 18) in this dataset.

Next, in order to gain more insight into associated functions, we performed DAVID Functional Annotation Clustering analysis. We found eight clusters significantly enriched in ST-cell, five in FrC-cell and three in ST-syn (Suppl. Table 5). Five of the ST-cell clusters are related to mitochondria (Enrichment Scores between 10.42 and 2.1).Two of the FrC-cell cluster are related to the proteasome (Enrichment Scores 4.5 and 1.7). Among the other enriched cluster are calmodulin-binding, microtubule, and synapse.

Subsequently, in order to investigate the underlying mechanism and cascades that may explain the observed DAPs, we tested whether the genes encoding DAPs were enriched for transcription factor binding. We found enrichment for 33 unique transcription factors (Suppl. Table 6**).** Six of the transcription factors are enriched more than once: TAF1 (FrC-cell and HC-syn), ATF2 (FrC-cell and HC-syn), CEBPD (FrC-cell amd HC-syn), NELFE (Frc-cell and HC-syn), PBX3 (FrC-cell and HC-syn) and REST (FrC-cell, ST-cell and ST-syn).

3.3. DAPs are enriched for schizophrenia risk

We hypothesized that DAPs, like BRD1 target genes and differentially expressed genes in mouse brains (Qvist et al., 2016; Fryland et al., 2016; Rajkumar et al., 2018), are enriched for psychiatric disorder risk genes. Because the strongest evidence for genetic association is found between SZ and *BRD1*, we first tested whether DAPs are enriched for SZ risk using MAGMA (de Leeuw et al., 2015). We found that DAPs from FrC-cell and HC-cell are significantly enriched for SZ risk ($p_{FrC-cell}$ = 0.049 and $p_{HC.cell}$ = 2.6E-5) (Fig. 3**).** Next, we investigated the enrichment of for mental health risk genes among DAPs, testing 7 other GWAS datasets, comprising 5 psychiatric disorders and 2 unrelated phenotypes **(Suppl. Information 6**).

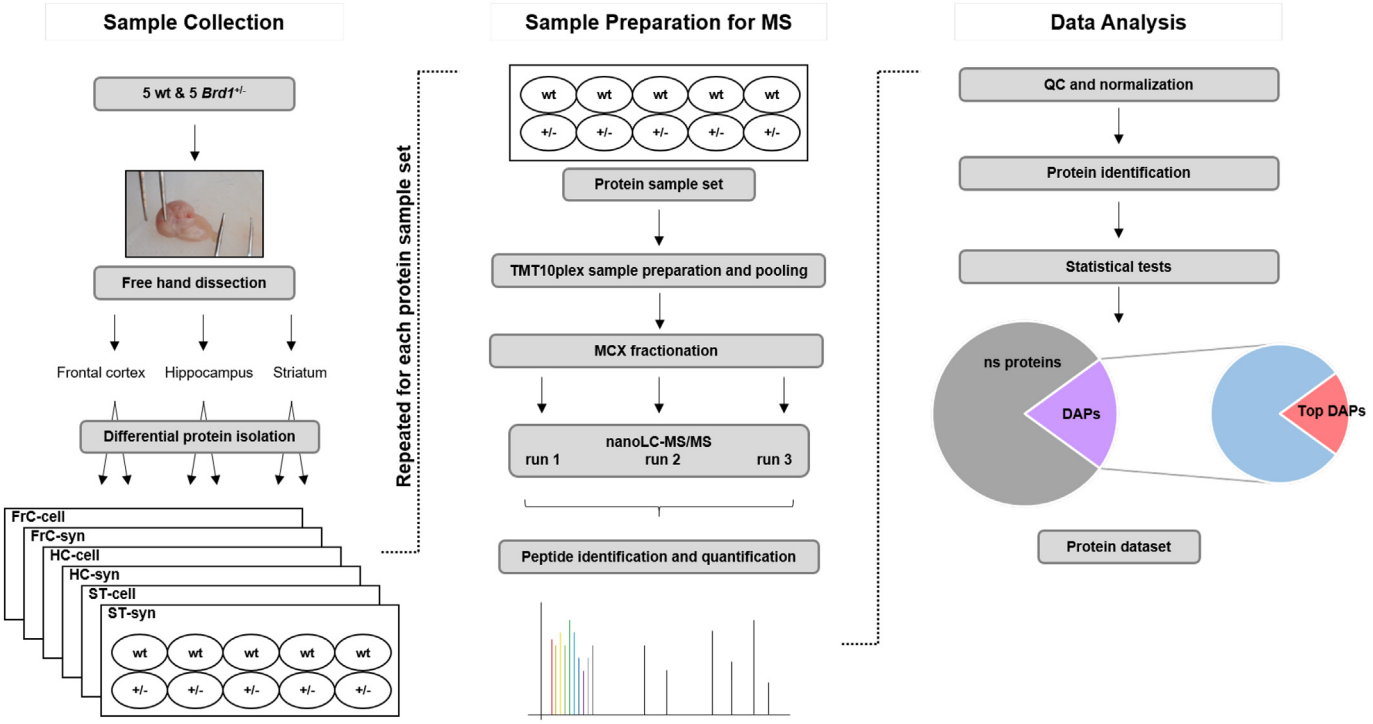

Fig. 1. Overview of the sample preparations and MS pipeline. Abbreviations: wild type (wt); female heterozygous Brd1 knockout mice (Brd1$^{+/-}$); frontal cortex (FrC); hippocampus (HC); striatum (ST); cell lysate (cell); synaptosome (syn); mass spectrometry (MS); mixed-mode cationic exchange (MCX); nano liquid chromatography – tandem mass spectrometry (nanoLC-MS/MS); quality control (QC); not significant (ns); differentially abundant proteins (DAPs); top differentially abundant proteins (top DAPs).

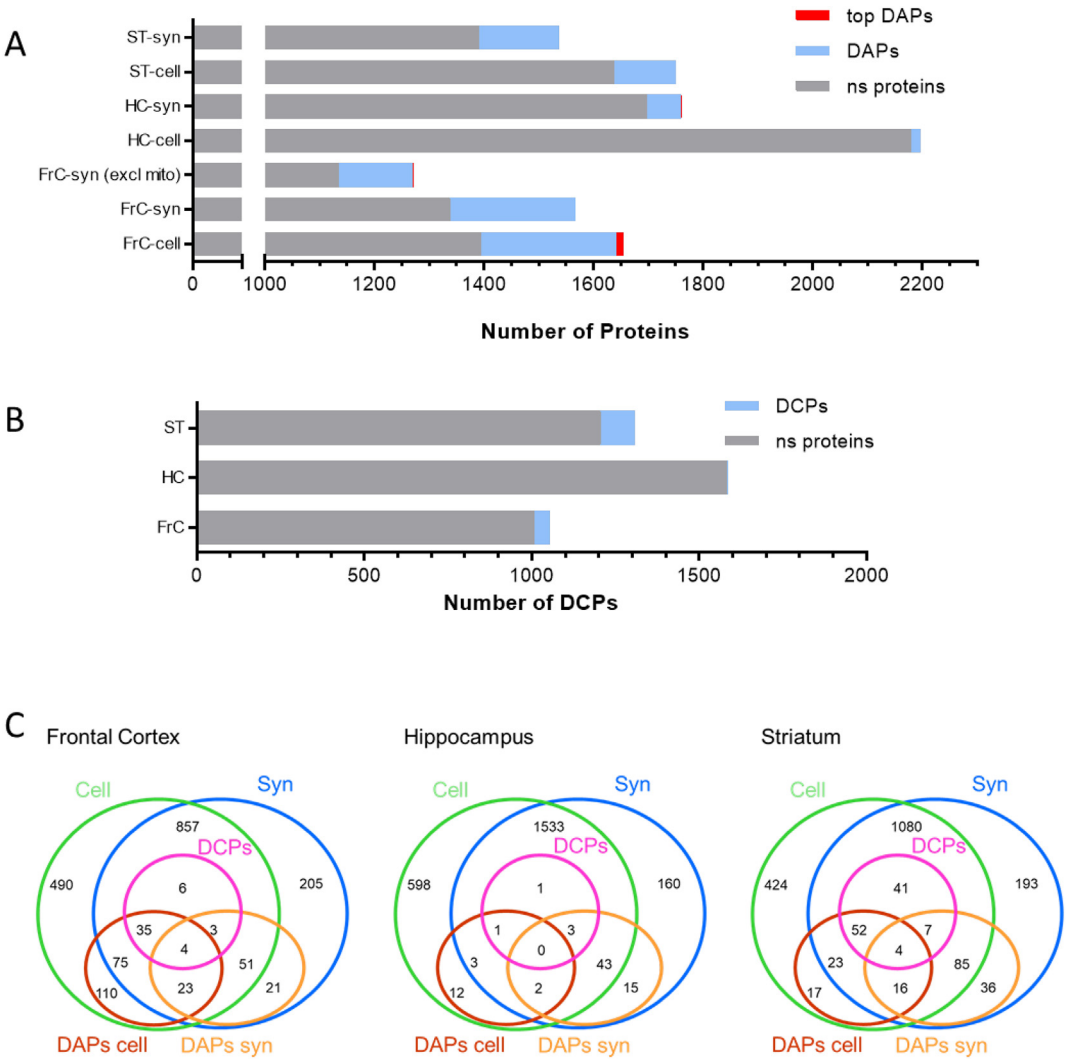

Fig. 2. A) Total number of unique proteins detected in female Brd1$^{+/-}$ mouse brain regions. Differentially abundant proteins (DAPs, $p < .05$ and LFC > cut-off); top differentially abundant proteins (Top DAPs $p < .001$ and LFC > cut-off). LFC cut-off: ± 0.231 (FrC-Cell), ± 0.104 (FrC-Syn), ± 0.099 (FrC-Syn (excl mito)), ± 0.191 (HC-Cell), ± 0.072 (HC-Syn), ± 0.189 (ST-Cell), ± 0.102 (ST-Syn). B) Total number of unique proteins shared between cell lysate and synaptosomal preparations of the same brain region and differentially compartmentalized proteins (DCPs, $p < .05$). **C)** Distribution of the proteins among fractions and statistical significant groups. Abbreviations: frontal cortex (FrC); hippocampus (HC); striatum (ST); cell lysate (cell); synaptosome (syn); not significant (ns).

3.4. BRD1 deficiency is associated with differential protein compartmentalization

Next we wondered whether we could identify differences in protein abundancy between the cell lysate and synaptosomal preparations, indicating that certain proteins are affected by processes such as trafficking or local protein degradation resulting in differential compartmentalization. To do so, we calculated the synaptosome-to-cell lysate abundancy ratio (syn/cell) for all proteins detected in both datasets from the same region ($n_{FrC} = 1054$, $n_{HC} = 1586$, $n_{ST} = 1308$) and compared these ratios between genotypes (Fig. 2B and C). We identified 48, 5 and 104 differentially compartmentalized proteins (DCPs) in FrC, HC and ST, respectively, when comparing genotypes (Suppl. Table 7). The vast majority of these (40/48 in FrC, 3/5 in HC and 99/104 in ST) of these have a negative LFC, indicating that these proteins are relatively less abundant in synaptosomal preparations compared to cell lysate in Brd1$^{+/-}$ mice. In line with this finding, several of the DCPs had been identified as DAPs (Fig. 2C). In FrC, 39 DCPs were also DAPs (37 upregulated) in cell lysate, and 7 were DAPs (5 downregulated) in synaptosome. Among the 5 DCPs in HC, we identified 1 DAP (upregulated) from cell lysate and 3 DAPs (1 downregulated) from synaptosome. In ST, 56 DAPs (54 upregulated) from cell lysate were among the DCPs, and 11 (6 downregulated) from synaptosome. We then used DAVID Functional Annotation Clustering analysis to identify the function of DCPs. This analysis revealed 1 cluster (enrichment score = 2.0) related to calcium signaling among DCPs in FrC, none in HC and 10 enriched clusters among DCPs in ST (enrichment scores between 1.4 and 13.7). Eight out of ten DCP clusters in ST were related to mitochondria.

3.5. BRD1 deficiency is associated with changes in dendritic spine morphology

We note that recurrent results point in the direction of aberrant neuromorphology in *Brd1*$^{+/-}$ mice: 1) Four top DAPs (OGFR, S100A5, MT3, GAP43) in this study have a function related to neuronal morphology and growth 2) DAVID cluster analysis of DAPs showed "microtubule" among the enriched clusters for the FrC-cell dataset, including DAPs like Tau, Microtubule-associated Protein 4 (MAP4) and Microtubule-associated protein 2 (MAP2); microtubule dynamics have been shown to influence dendritic spine morphology (Penazzi et al., 2016; Dent, 2017) and 3) We have previously reported altered

Table 1
Overview of the top differential abundant proteins (top DAPs) detected in female Brd1$^{+/-}$ mouse brain.

UniProt entry name[1]	Gene Symbol	UniProt protein name	P-value	LFC	Dataset
Transcription & chromatin					
TB182_MOUSE	Tnks1bp1	182 kDa tankyrase-1-binding protein	0.0003	0.70	Frc-cell
TMA7_MOUSE	Tma7	Translation machinery-associated protein 7	0.0003	0.93	Frc-cell
TCAL5_MOUSE	Tceal5	Transcription elongation factor A protein-like 5	0.0004	1.05	Frc-cell
HMGN1_MOUSE	Hmgn1	Non-histone chromosomal protein HMG-14	0.0005	0.82	Frc-cell
T22D1_MOUSE	Tsc22d1	TSC22 domain family protein 1	0.0005	0.92	Frc-cell
CNBP_MOUSE	Cnbp	Cellular nucleic acid-binding protein	0.0010	0.75	Frc-cell
Cellular transport					
SYNRG_MOUSE	Synrg	Synergin gamma	0.0008	0.79	Frc-cell
MON2_MOUSE	Mon2	Protein MON2 homolog	0.0006	0.53	HC-syn
Neuroendocrine					
CMGA_MOUSE	Chga	Chromogranin-A	0.0004	1.05	Frc-cell
PENK_MOUSE	Penk	Proenkephalin-A	0.0004	0.85	Frc-cell
Neuronal morphology and growth					
OGFR_MOUSE	Ogfr	Opioid growth factor receptor	0.0005	0.93	Frc-cell
S10A5_MOUSE	S100a5	Protein S100-A5	0.0007	−0.67	Frc-syn
MT3_MOUSE	Mt3	Metallothionein-3	0.0008	1.07	Frc-cell
NEUM_MOUSE	Gap43	Neuromodulin	0.0002	0.47	Frc-syn
Other					
PTMA_MOUSE	Ptma	Prothymosin alpha	0.0005	1.12	Frc-cell
PRC2C_MOUSE	Prrc2c	Protein PRRC2C	0.0007	0.56	Frc-cell

The listed proteins passed the criteria of both $p < .001$ and log2 fold change (LFC > cut-off). LFC: log2 fold change compared to WT mice. Abbreviations: Frontal cortex (FrC); hippocampus (HC); striatum (ST); cell lysate (cell); synaptosome (syn)

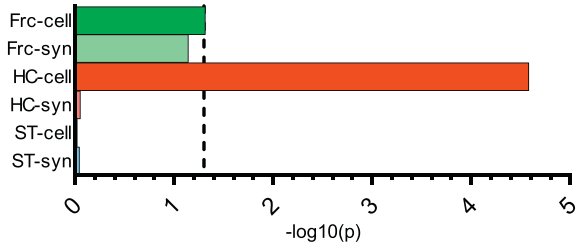

Fig. 3. MAGMA disease risk enrichment analysis for schizophrenia. Black dashed line: significance threshold ($p = .05$). Abbreviations: frontal cortex (FrC); hippocampus (HC); striatum (ST); cell lysate (cell); synaptosome (syn).

morphology of pyramidal neurons in the aCC of female *Brd1*$^{+/-}$ mice (Rajkumar et al., 2018). We hypothesized here that dendritic spine morphology in addition is altered in *Brd1*$^{+/-}$ mouse brain, and performed a morphology analysis of dendritic spines derived from aCC pyramidal neurons.

We first classified the spines into 4 classes (stubby, mushroom, long thin and filopodia) and observed an overall difference in distribution between genotypes (Chi square test, $p < .001$) (Fig. 4A). This overall difference seems to be driven by a loss of mushroom types (−5.2%) and a gain of stubby type spines (+4.3%) in *Brd1*$^{+/-}$ mice. To determine the underlying differences between genotypes that cause this class shift, we measured spine length, area, volume, minimum and maximum diameter for the whole dendritic spine as well as for the subparts spine head, neck and ground (the subparts not for spine area) from the same dendritic spines. After correcting for multiple testing, we found that dendritic spines from *Brd1*$^{+/-}$ mice were smaller with respect to minimum (total spine, $p_{adjusted} < 0.0001$, $\beta_{logodds} = -28.8 \pm 2.1$) and maximum (total spine, $p_{adjusted} = 0.01216$, $\beta_{logodds} = -4.8 \pm 1.5$) diameter for the total spine, spine head, neck and ground (Fig. 4B, C, and Suppl. Table 8). The observed differences in maximum diameter and maximum ground diameter was found in the smaller subpopulation (spines with diameter ≤ 234.0 nm), but not in the larger subpopulation (Suppl. Table 8). Additionally, spines with length < 1.2 µm were significantly smaller in *Brd1*$^{+/-}$ mice ($p_{adjusted} = 0.01391$, $\beta = -48.3 \pm 16.6$ nm) (Fig. 4D). Fig. 4E illustrates and summarizes the effects of reduced *Brd1* levels on pyramidal neuron spine morphology in aCC.

4. Discussion

In this study, we use proteomic profiling to demonstrate widespread changes in protein abundancies and compartmentalization in brain regions of female *Brd1*$^{+/-}$ mice. We found that affected proteins are highly interconnected and they cluster in functions related to transcription and chromatin, in line with the putative role of BRD1 as a scaffold protein in HAT complexes(Fryland et al., 2016; Mishima et al., 2011), as well as mitochondria and the cytoskeleton. Directly based on these findings, we studied dendritic spines in aCC and found evidence of aberrant morphology. Upstream of DAPs, we found enrichment for several transcription factors. In line with the current and previous findings that proteins important for mitochondrial function are regulated upon reduced BRD1 levels in mouse brain regions (Rajkumar et al., 2018), the PPARD transcription factor is involved in the nuclear control of proteins important for mitochondrial function. Of specific interest with respect to previous findings are CREB1 and SMAD4, the latter found in complexes with among others c-FOS. In male *Brd1*$^{+/-}$ mice, CREB has been identified as an likely upstream regulator of differentially expressed genes in striatum and aCC and has been found hyperphosphorylated in whole brain extracts (Qvist et al., 2016). Its transcriptional target, c-FOS, was furthermore significantly more abundant in the same samples (Qvist et al., 2016). Of special note, we found enrichment for schizophrenia risk among identified DAPs in frontal cortex and hippocampus further supporting the functional link between BRD1 and schizophrenia risk genes (Qvist et al., 2016; Fryland et al., 2016; Rajkumar et al., 2018). In close analogy to the experimental setup in the present study, review-analyses of proteomic studies of *post-mortem* brain tissue from patients with SZ and BD have further revealed that, indifferent for the used platform or studied brain region, mitochondrial and cytoskeletal components are consistently dysregulated (English et al., 2011; Saia-cereda et al., 2017; Davalieva et al., 2016).

Previously we have shown that the reduced expression of *Brd1* leads to phenotypes with translational relevance to SZ in mice, including many aspects from positive, negative and cognitive symptoms (Qvist et al., 2016; Rajkumar et al., 2018; Qvist et al., 2017). In the present

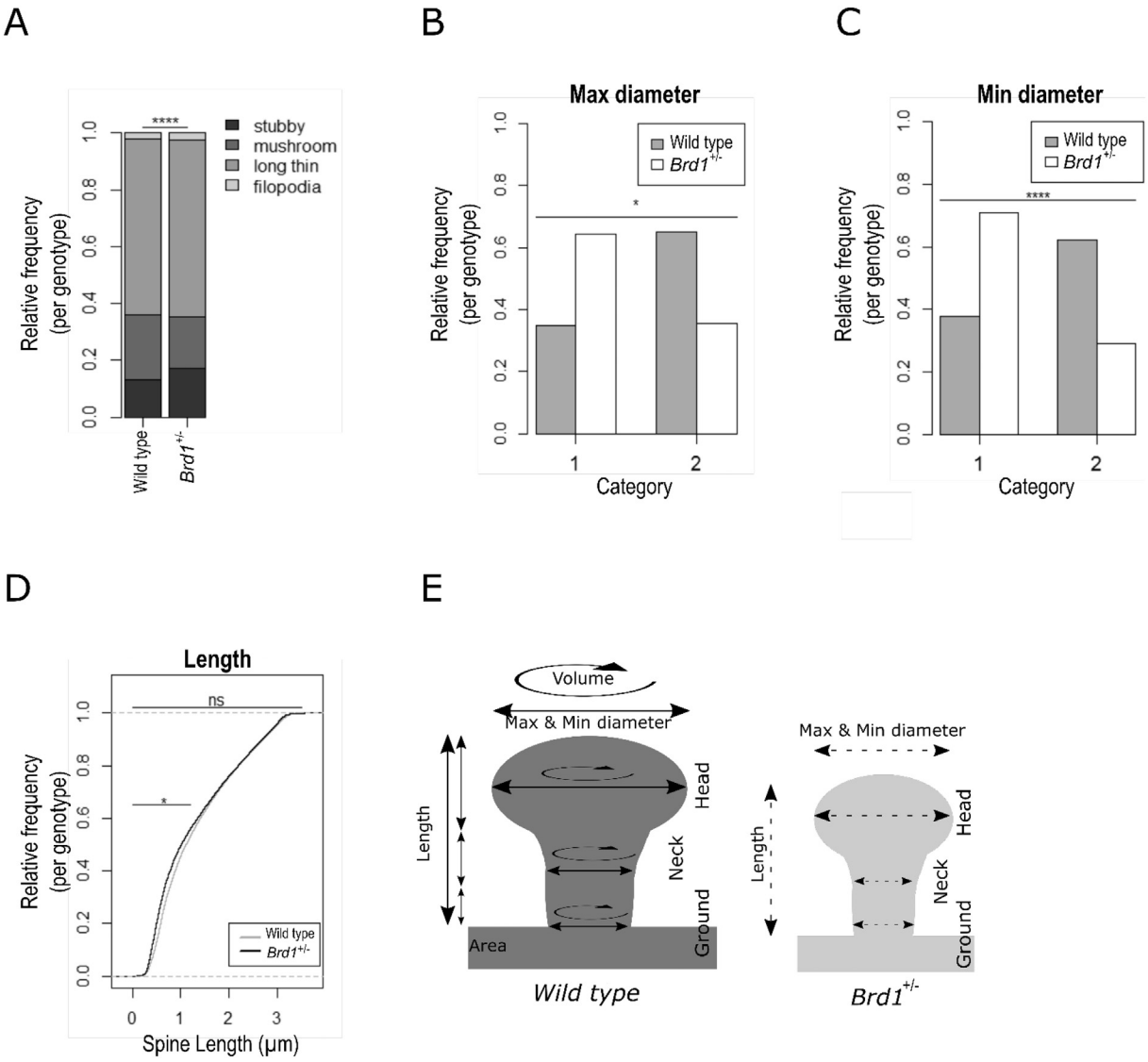

Fig. 4. Analysis of dendritic spine morphology in aCC pyramidal neurons. A) Relative distribution of 4 dendritic spine types. B) Comparison of relative frequency per genotype of maximum diameter of dendritic spines per category (category 1: maximum spine diameter < 117.0 nm, category 2: 117.0 nm ≤ maximum spine diameter) between wild type (n = 27,182) and Brd1$^{+/-}$ (n = 11,820) spines. *P*-value as determined using a generalized linear mixed-effect model. C) Comparison of relative frequency of minimum diameter of dendritic spines per category (category 1: minimum spine diameter < 117.0 nm, category 2: 117.0 nm ≤ minimum spine diameter ≤ 234.0 nm) between wild type and Brd1$^{+/-}$ dendritic spines. P-value as determined using a generalized linear mixed-effect model. D) Comparison of the cumulative frequency of spine length between wild type and Brd1$^{+/-}$ spines. P-value as determined using a linear mixed-effect model. Small spines are defined as spines with spine length < 1.2 µm. E) Overview of measured parameters and comparison between dendritic spines derived from wild type and Brd1$^{+/-}$ mice. Dotted line represents parameters with a significant difference between genotypes. Ns: not significant, * p < .05, **** p < .001.

study, we profiled BRD1 dependent changes in protein abundancies and compartmentalization in mouse brain to further decipher the potential impact of its deficiency. Proteomic profiles represent the true state of the cell better than transcriptomic profiles, as they assess the final sum of protein synthesis, degradation and localization. On the other hand, researchers in proteomics have to compromise between sensitivity and risk for false positives, therefore tending to be rather conservative, and face limited coverage of low abundant proteins (Sidoli et al., 2016) and limited sample size in the case of quantification based on isobaric labelling. To deal with low coverage, we employed the combination of distinct sample preparation, each enriching for proteins from different cell compartments, as well was repeated measurement of the same samples with different LC-MS/MS settings. To avoid false positives, we employed a rather conservative approach during QC, only including MS scans, peptides and proteins with sufficient evidence in the final datasets.

Both cytoskeleton dynamics and mitochondria are known to influence neuronal and dendritic spine morphology. Firstly, spine morphology is regulated tightly by both the F-actin and microtubule network. F-actin is mostly located within the spine, whereas microtubule provide a dynamic support for transport both long-distance and activity-dependent transport of cargoes in and out the spine (Dent, 2017). Inadequate functioning of the cytoskeleton dynamics could lead to aberrant spine morphology and to disease. For example, drug-induced destabilization of microtubule modulated spine morphology from the mature mushroom-type into the immature filopodia-type (Jaworski et al., 2009), knockout of PAR1B in mice reduced the number of mature spines and induced spatial memory formation (Segu et al., 2008). Furthermore, decreased immunoreactivity of MAP2 has been repeatedly shown in *post-mortem* brains from SZ patients and is associated with reduced spine density (Shelton et al., 2015).

Secondly, besides their well-known function in energy metabolism,

calcium homeostasis, production of reactive oxygen species (ROS) and apoptosis, mitochondria play an essential role in regulating neurogenesis and neuronal plasticity (Morava & Kozicz, 2013). Disruption of mitochondrial protein translation in *Drosophila* neurons, reduced dendritic arborization, but axon morphology remained relatively unchanged (Chihara et al., 2007), which is similar to the aberrant pyramidal neuronal morphology observed in female *Brd1*$^{+/-}$ mice (Rajkumar et al., 2018). The differences in fold change ratios of mitochondrial proteins between cell lysate and synaptosome purification from the same brain region that we find in the present study could be indicative for altered mitochondrial morphology in female *Brd1*$^{+/-}$ mice, as the filtration steps during the synaptosome preparation favor the extraction of smaller mitochondria. Interestingly, presynaptic mitochondrial morphology has been shown to correlate with impaired working memory in monkey brain (Hara et al., 2014). Moreover, the mitochondrial apoptotic pathway can be moderately and locally activated to induce LTD, resulting in shrinkage and loss of dendritic spines in the absence of cell death (Sheng & Ertürk, 2014; D'Amelio et al., 2011). This system as well as mitochondria morphological changes are sensitive to sublethal mitochondrial stress (D'Amelio et al., 2011; Barbour & Turner, 2014), which can be induced by excess of Ca^{2+} through disinhibition of glutamate release as a result of GABAergic dysfunction or by loss of Ca^{2+} buffering capacity through loss of parvalbumin (Davis et al., 2014), both observed in *Brd1*$^{+/-}$ mice (Qvist et al., 2016). Finally, mitochondrial function has been shown to be linked to synaptic plasticity, cell resilience and psychiatric phenotypes (Manji et al., 2012; Palmfeldt et al., 2016). Mitochondrial genes are in fact significantly enriched among the 108 schizophrenia genome-wide associated loci (Hjelm et al., 2015) and psychiatric disorders are comorbid to mitochondrial dysfunction and can be diagnosed years before any symptoms of mitochondrial disease (Anglin et al., 2012; Fattal et al., 2007).

When we investigated dendritic spine morphology in aCC from female *Brd1*$^{+/-}$ mice, we found that reduced *Brd1* levels coincide with a loss of the mature mushroom-type and an increase of the immature stubby spines (Qiao et al., 2016). Furthermore, dendritic spines in *Brd1*$^{+/-}$ mice are generally smaller, and this is especially pronounced in the small spines subgroup. Whereas the spine head size is directly correlated to the post synaptic density size, presynaptic vesicle amount (Harris ' et al., 1989) and postsynaptic receptor abundance (Noguchi et al., 2005; Matsuzaki et al., 2001), reduced neck and ground diameter have been shown to greatly limit the signal transduction and diffusion rates of molecules into the dendritic shaft (Noguchi et al., 2005; Ramirez et al., 2015). Under normal circumstances, small spines with thin necks are more likely to limit efflux from the spine head and, hereby making them more optimized for selective induction of long term potentiation (LTP) (Noguchi et al., 2005), and large spines are more resistant to LTP hereby securing memory formation (Matsuzaki et al., 2004). On the other hand, Ca^{2+} spread from the dendritic spine into the dendritic shaft and neighboring spines contributes to the potentiation and stabilization of co-active spines during development of the brain (Lee et al., 2016). Similarly, in the adult brain Rho GTPases can diffuse to neighboring spines and change the conditions for LTP or long term depression (LTD) locally, greatly influencing the establishment and maintenance of neuronal networks (Govindarajan et al., 2011; van Bommel & Mikhaylova, 2016). The smaller spines could therefore suggest memory formation impairments as observed in both male and female *Brd1*$^{+/-}$ mice (Qvist et al., 2016; Rajkumar et al., 2018; Qvist et al., 2017).

5. Conclusion

In summary, we show that reduced BRD1 levels have widespread effects on protein abundancies and compartmentalization in mouse brain regions. Further linking the actions of BRD1 to psychiatric disorders, we find that affected proteins in frontal cortex and hippocampus are enriched for schizophrenia risk. Our study also principally corroborate previous indications from RNAseq studies in *Brd1*$^{+/-}$ mice that reduced *Brd1* expression in mouse brain might disturb mitochondrial function and cytoskeletal organization, both of which have been shown to play a role in neuromorphology, as well as density and morphology of spines. Lastly, we show that female *Brd1*$^{+/-}$ mice display reduced dendritic spine size, which is likely to affect memory formation and inhibit clustered spine plasticity, affecting brain network formation and information processing. Future studies using for example two photon microscopy investigating live spine response to stimuli and the effect of malformed spines on spine crosstalk could supplement our data and help us identify the role of BRD1 in these brain processes.

Supplementary data to this article can be found online at https://doi.org/10.1016/j.nbd.2018.12.011.

Acknowledgements

This study was funded by the Lundbeck Foundation, Denmark (grant number R155-2014-1724) (ADB), The Novo Nordisk Foundation (ADB & JHC), The Danish Council for Independent Research–Medical Sciences (ADB and JHC), Aarhus University (ADB) and John and Birthe Meyer Foundation (JhP). Centre for Stochastic Geometry and Advanced Bioimaging is supported by Villum Foundation. The funders had no involvement in any aspect of the study.

We thank Anne Hedemand (Aarhus University) and Tanja Østergaard (Aarhus University) for genotyping of mice, Margrethe Kjeldsen (Aarhus University Hospital) and Tanja Østergaard (Aarhus University) for assistance with Western Blotting and Abdel-Rahman Al-Absi (Aarhus University Hospital) for assistance with dendritic spine morphology analysis.

Contributions

VP, MS, APR, GW, JRN, JhP, ADB, JHC designed and directed experiments. VP, MS, APR collected samples and data. VP, MS, AVE, EAE, JhP analyzed mass spectrometry results. VP, MS, APR, JG, JhP, ADB, JHC performed statistical analysis. JnP performed MAGMA analysis. VP, APR, JG, GW, JRN, JHC designed, performed and analyzed spine morphology experiments. VP, MS, PQ, TF, JhP, ADB, JHC interpreted results. VP wrote the first draft of the manuscript. All authors contributed to the finalization of the manuscript.

Conflict of interest

OM and ADB are co-inventors on a patent application submitted by Aarhus University entitled “Method for diagnosis and treatment of a mental disease” (EP2287340) that includes claims relating to BRD1 among other genes. OM, ADB, JHC, APR, and PQ are coinventors on a patent application submitted by Capnova A/S entitled “Genetically modified non-human mammal and uses thereof” (PCT/EP2013/069524) that includes the *Brd1*$^{+/-}$ mouse.

The other authors declare no conflict of interest.

References

Andreassen, O.A., Thompson, W.K., Dale, A.M., 2014. Boosting the power of schizophrenia genetics by leveraging new statistical tools. Schizophr. Bull. 40, 13–17.

Anglin, R.E., Tarnopolsky, M.A., Mazurek, M.F., Rosebush, P.I., 2012. The psychiatric presentation of mitochondrial disorders in adults. J. Neuropsychiatr. Clin. Neurosci. 24, 394–409.

Barbour, J.A., Turner, N., 2014. Mitochondrial stress signaling promotes cellular adaptations. Int. J. Cell Biol. 2014, 156020.

van Bommel, B., Mikhaylova, M., 2016. Talking to the neighbours: the molecular and physiological mechanisms of clustered synaptic plasticity. Neurosci. Biobehav. Rev. 71, 352–361.

Brosch, M., Yu, L., Hubbard, T., Choudhary, J., 2009. Accurate and sensitive peptide identification with Mascot Percolator. J. Proteome Res. 8, 3176–3181.

Chang, J.W., Arnold, M.M., Rozenbaum, A., Caputo, A., Schweizer, F.E., Huynh, M., et al., 2012. Synaptoneurosome micromethod for fractionation of mouse and human brain,

and primary neuronal cultures. J. Neurosci. Methods 211, 289–295.
Chen, E.Y., Tan, C.M., Kou, Y., Duan, Q., Wang, Z., Meirelles, G.V., et al., 2013. Enrichr: interactive and collaborative HTML5 gene list enrichment analysis tool. BMC Bioinformatics 14, 128.
Chihara, T., Luginbuhl, D., Luo, L., 2007. Cytoplasmic and mitochondrial protein translation in axonal and dendritic terminal arborization. Nat. Neurosci. 10, 828–837.
Cho, H.I., Kim, M.S., Jang, Y.K., 2016. The BRPF2/BRD1-MOZ complex is involved in retinoic acid-induced differentiation of embryonic stem cells. Exp. Cell Res. 346. https://doi.org/10.1016/j.yexcr.2016.05.022.
Christensen, J.H., Elfving, B., Müller, H.K., Fryland, T., Nyegaard, M., Corydon, T.J., et al., 2012. The Schizophrenia and Bipolar Disorder associated BRD1 gene is regulated upon chronic restraint stress. Eur. Neuropsychopharmacol. 22, 651–656.
Cross-Disorder, 2013. Group of the Psychiatric Genomics Consortium. Identification of risk loci with shared effects on five major psychiatric disorders: a genome-wide analysis. Lancet 381, 1371–1379.
D'Amelio, M., Cavallucci, V., Middei, S., Marchetti, C., Pacioni, S., Ferri, A., et al., 2011. Caspase-3 triggers early synaptic dysfunction in a mouse model of Alzheimer's disease. Nat. Neurosci. 14, 69–76.
Davalieva, K., Maleva Kostovska, I., Dwork, A.J., 2016. Proteomics Research in Schizophrenia. Front. Cell. Neurosci. 10, 18.
Davis, J., Moylan, S., Harvey, B.H., Maes, M., Berk, M., 2014. Neuroprogression in schizophrenia: pathways underpinning clinical staging and therapeutic corollaries. Aust. New Zeal J. Psych. 48, 512–529.
Demontis, D., Walters, R.K., Martin, J., Mattheisen, M., Als, T.D., Agerbo, E., et al., 2019. Discovery of the first genome-wide significant risk loci for attention deficit/hyperactivity disorder. Nat. Genet. 51, 63–75 (145581).
Dent, E.W., 2017. Of microtubules and memory: implications for microtubule dynamics in dendrites and spines. Mol. Biol. Cell 28, 1–8.
Dyrvig, M., Qvist, P., Lichota, J., Larsen, K., Nyegaard, M., Børglum, A.D., et al., 2017. DNA methylation analysis of BRD1 promoter regions and the Schizophrenia rs138880 risk Allele. PLoS One 12, e0170121.
English, J.A., Pennington, K., Dunn, M.J., Cotter, D.R., 2011. The neuroproteomics of schizophrenia. Biol. Psychiatry 69, 163–172.
Fattal, O., Link, J., Quinn, K., Cohen, B.H., Franco, K., 2007. Psychiatric comorbidity in 36 adults with mitochondrial cytopathies. CNS Spectr. 12, 429–438.
Fryland, T., Elfving, B., Christensen, J.H., Mors, O., Wegener, G., Børglum, A.D., 2012. Electroconvulsive seizures regulates the Brd1 gene in the frontal cortex and hippocampus of the adult rat. Neurosci. Lett. 516, 110–113.
Fryland, T., Christensen, J.H., Pallesen, J., Mattheisen, M., Palmfeldt, J., Bak, M., et al., 2016. Identification of the BRD1 interaction network and its impact on mental disorder risk. Genome Med. 8, 53.
Genomes Project Consortium, Abecasis, G.R., Auton, A., Brooks, L.D., DePristo, M.A., Durbin, R.M., et al., 2012. An integrated map of genetic variation from 1,092 human genomes. Nature 491, 56–65.
Govindarajan, A., Israely, I., Huang, S.-Y., Tonegawa, S., 2011. The Dendritic branch is the preferred integrative unit for protein synthesis-dependent LTP. Neuron 69, 132–146.
Grove, J., Ripke, S., Als, T.D., Mattheisen, M., Walters, R., Won, H., et al., 2017. Common risk variants identified in autism spectrum disorder. bioRxiv, 224774.
Hara, Y., Yuk, F., Puri, R., Janssen, W.G.M., Rapp, P.R., Morrison, J.H., 2014. Presynaptic mitochondrial morphology in monkey prefrontal cortex correlates with working memory and is improved with estrogen treatment. Proc. Natl. Acad. Sci. U. S. A. 111, 486–491.
Harris ', K.M., Stevens, J.K., Harris, K.M., 1989. Dendritic spines of CA1 pyramidal cells in the Rat Hippocampus: serial electron microscopy with reference to their biophysical characteristics. J. Neurosci. 2982–2997.
Hjelm, B.E., Rollins, B., Mamdani, F., Lauterborn, J.C., Kirov, G., Lynch, G., et al., 2015. Evidence of Mitochondrial dysfunction within the complex genetic etiology of Schizophrenia. Mol. Neuropsych. 1, 201–219.
Huang, D.W., Sherman, B.T., Lempicki, R.A., 2009. Systematic and integrative analysis of large gene lists using DAVID bioinformatics resources. Nat. Protoc. 4, 44–57.
Jaworski, J., Kapitein, L.C., Gouveia, S.M., Dortland, B.R., Wulf, P.S., Grigoriev, I., et al., 2009. Dynamic microtubules regulate Dendritic spine morphology and synaptic plasticity. Neuron 61, 85–100.
Jorgensen, T.H., Børglum, a.D., Mors, O., Wang, a.G., Pinaud, M., Flint, T.J., et al., 2002. Search for common haplotypes on chromosome 22q in patients with schizophrenia or bipolar disorder from the Faroe Islands. Am. J. Med. Genet. – Neuropsychiatr. Genet. 114, 245–252.
Aberg, K.A., Liu, Y., Bukszár, J., McClay, J.L., Khachane, A.N., Andreassen, O.A., et al., 2013. A comprehensive family-based replication study of schizophrenia genes. JAMA Psychiatry 70, 573–581.
Kuznetsova, A., Brockhoff, P.B., Christensen, R.H.B., 2016. lmerTest: Tests in Linear Mixed Effects Models.
Lambert, J.C., Ibrahim-Verbaas, C.A., Harold, D., Naj, A.C., Sims, R., Bellenguez, C., et al., 2013. Meta-analysis of 74,046 individuals identifies 11 new susceptibility loci for Alzheimer's disease. Nat. Genet. 45, 1452–1458.
Lee, K.F.H., Soares, C., Thivierge, J.-P., Béïque, J.-C., 2016. Correlated synaptic inputs drive Dendritic calcium amplification and cooperative plasticity during clustered synapse development. Neuron 89, 784–799.
de Leeuw, C.A., Mooij, J.M., Heskes, T., Posthuma, D., 2015. MAGMA: generalized gene-set analysis of GWAS data. PLoS Comput. Biol. 11, e1004219.
Lek, M., Karczewski, K.J., Minikel, E.V., Samocha, K.E., Banks, E., Fennell, T., et al., 2016. Analysis of protein-coding genetic variation in 60,706 humans. Nature 536, 285–291.
Major Depressive Disorder Working Group of the Psychiatric GWAS Consortium, Ripke, S., Wray, N.R., Lewis, C.M., Hamilton, S.P., Weissman, M.M., et al., 2013. A mega-analysis of genome-wide association studies for major depressive disorder. Mol. Psychiatry 18, 497–511.
Manji, H., Kato, T., Di, Prospero N.a., Ness, S., Beal, M.F., Krams, M., et al., 2012. Impaired mitochondrial function in psychiatric disorders. Nat. Rev. Neurosci. 13, 293–307.
Matsuzaki, M., Ellis-Davies, G.C.R., Nemoto, T., Miyashita, Y., Iino, M., Kasai, H., 2001. Dendritic spine geometry is critical for AMPA receptor expression in hippocampal CA1 pyramidal neurons. Nat. Neurosci. 4, 1086–1092.
Matsuzaki, M., Honkura, N., Ellis-Davies, G.C.R., Kasai, H., 2004. Structural basis of long-term potentiation in single dendritic spines. Nature 761–766.
Mishima, Y., Miyagi, S., Saraya, A., Negishi, M., Endoh, M., Endo, T.A., et al., 2011. The Hbo1-Brd1/Brpf2 complex is responsible for global acetylation of H3K14 and required for fetal liver erythropoiesis. Blood 118, 2443–2453.
Morava, E., Kozicz, T., 2013. Mitochondria and the economy of stress (mal)adaptation. Neurosci. Biobehav. Rev. 37, 668–680.
Mudunuri, U., Che, A., Yi, M., Stephens, R.M., 2009. bioDBnet: the biological database network. Bioinformatics 25, 555–556.
Noguchi, J., Matsuzaki, M., Ellis-Davies, G.C.R., Kasai, H., 2005. Spine-neck geometry determines NMDA receptor-dependent Ca2+ signaling in dendrites. Neuron 46, 609–622.
Nyegaard, M., Severinsen, J.E., Als, T.D., Hedemand, A., Straarup, S., Nordentoft, M., et al., 2010. Support of association between BRD1 and both schizophrenia and bipolar affective disorder. Am. J. Med. Genet. Part B Neuropsychiatry Genet. 153, 582–591.
Pagliarini, D.J., Calvo, S.E., Chang, B., Sheth, S.A., Vafai, S.B., Ong, S.-E., et al., 2008. A mitochondrial protein compendium elucidates complex I disease biology. Cell 134, 112–123.
Palmfeldt, J., Henningsen, K., Eriksen, S.A., Müller, H.K., Wiborg, O., 2016. Protein biomarkers of susceptibility and resilience to stress in a rat model of depression. Mol. Cell. Neurosci. 74, 87–95.
Pardiñas, A.F., Holmans, P., Pocklington, A.J., Escott-Price, V., Ripke, S., Carrera, N., et al., 2016. Common Schizophrenia Alleles Are Enriched in Mutation-Intolerant Genes and Maintained by Background Selection. https://doi.org/10.1101/068593.
Paternoster, V., Rajkumar, A.P., Nyengaard, J.R., Børglum, A.D., Grove, J., Christensen, J.H., 2017. The importance of data structure in statistical analysis of dendritic spine morphology. J. Neurosci. Methods 296, 93–98.
Pavelka, N., Pelizzola, M., Vizzardelli, C., Capozzoli, M., Splendiani, A., Granucci, F., et al., 2004. A power law global error model for the identification of differentially expressed genes in microarray data. BMC Bioinformatics 5, 203.
Pavelka, N., Fournier, M.L., Swanson, S.K., Pelizzola, M., Ricciardi-Castagnoli, P., Florens, L., et al., 2008. Statistical similarities between transcriptomics and quantitative shotgun proteomics data. Mol. Cell. Proteomics 7, 631–644.
Penazzi, L., Bakota, L., Brandt, R., 2016. Microtubule dynamics in neuronal development, plasticity, and neurodegeneration. Int. Rev. Cell Mol. Biol. 321, 89–169.
Polpitiya, A.D., Qian, W.-J.J., Jaitly, N., Petyuk, V.A., Adkins, J.N., Camp, D.G., et al., 2008. DAnTE: a statistical tool for quantitative analysis of -omics data. Bioinformatics 24, 1556–1558.
Psychiatric GWAS Consortium Bipolar Disorder Working Group, 2011. Large-scale genome-wide association analysis of bipolar disorder identifies a new susceptibility locus near ODZ4. Nat. Genet. 43, 977–983.
Purcell, S.M., Moran, J.L., Fromer, M., Ruderfer, D., Solovieff, N., Roussos, P., et al., 2014. A polygenic burden of rare disruptive mutations in schizophrenia. Nature 506, 185–190.
Qiao, H., Li, M.-X., Xu, C., Chen, H.-B., An, S.-C., Ma, X.-M., et al., 2016. Dendritic spines in depression: what we learned from animal models. Neural Plast. 2016, 1–26.
Qvist, P., Christensen, J.H., Vardya, I., Rajkumar, A.P., Mørk, A., Paternoster, V., et al., 2016. The Schizophrenia-associated BRD1 gene regulates behavior, neurotransmission, and expression of Schizophrenia risk enriched gene sets in mice. Biol. Psychiatry. https://doi.org/10.1016/j.biopsych.2016.08.037.
Qvist, P., Rajkumar, A.P., Redrobe, J.P., Nyegaard, M., Christensen, J.H., Mors, O., et al., 2017. Mice heterozygous for an inactivated allele of the schizophrenia associated Brd1 gene display selective cognitive deficits with translational relevance to schizophrenia. Neurobiol. Learn. Mem. 141, 44–52.
Qvist, P., Eskildsen, S.F., Hansen, B., Baragji, M., Ringgaard, S., Roovers, J., et al., 2018. Brain volumetric alterations accompanied with loss of striatal medium-sized spiny neurons and cortical parvalbumin expressing interneurons in Brd1+/− mice. Sci. Rep. 8, 16486.
Rajkumar, A.P., Qvist, P., Larsen, S.H., Lazarus, R., Pallesen, J., Nava, N., et al., 2018. The behavioral and neurobiological effects of reduced Brd1 expression in mice are sex-biased and implicate gender dependent dysregulation of nuclear receptor mediated signaling in mental disorders. bioRxiv 257170.
Ramirez, S.A., Raghavachari, S., Lew, D.J., 2015. Dendritic spine geometry can localize GTPase signaling in neurons. Mol. Biol. Cell 26, 4171–4181.
Ripke, S., Neale, B.M., Corvin, A., Walters, J.T.R., Farh, K.-H., Holmans, P.A., et al., 2014. Biological insights from 108 schizophrenia-associated genetic loci. Nature 511, 421–427.
Saia-Cereda, V.M., Cassoli, J.S., Martins-De-Souza, D., Nascimento, J.M., 2017. Psychiatric disorders biochemical pathways unraveled by human brain proteomics. Eur. Arch. Psychiatry Clin. Neurosci. 267, 3–17.
Segu, L., Pascaud, A., Costet, P., Darmon, M., Buhot, M.-C., 2008. Impairment of spatial learning and memory in ELKL motif Kinase1 (EMK1/MARK2) knockout mice. Neurobiol. Aging 29, 231–240.
Severinsen, J.E., Bjarkam, C.R., Kiaer-Larsen, S., Olsen, I.M., Nielsen, M.M., Blechingberg, J., et al., 2006. Evidence implicating BRD1 with brain development and susceptibility to both schizophrenia and bipolar affective disorder. Mol. Psychiatry 11, 1126–1138.
Shelton, M.A., Newman, J.T., Gu, H., Sampson, A.R., Fish, K.N., MacDonald, M.L., et al., 2015. Loss of microtubule-associated protein 2 immunoreactivity linked to Dendritic

spine loss in Schizophrenia. Biol. Psychiatry 78. https://doi.org/10.1016/j.biopsych.2014.12.029.
Sheng, M., Ertürk, A., 2014. Long-term depression: a cell biological view. Philos. Trans. R. Soc. Lond. Ser. B Biol. Sci. 369, 20130138.
Sidoli, S., Kulej, K., Garcia, B.A., 2016. Why proteomics is not the new genomics and the future of mass spectrometry in cell biology. J. Cell Biol. https://doi.org/10.1083/jcb.201612010.
Smith, A.C., Blackshaw, J.A., Robinson, A.J., 2012. MitoMiner: a data warehouse for mitochondrial proteomics data. Nucleic Acids Res. 40, D1160–D1167.
Szklarczyk, D., Franceschini, A., Wyder, S., Forslund, K., Heller, D., Huerta-Cepas, J., et al., 2015. STRING v10: protein-protein interaction networks, integrated over the tree of life. Nucleic Acids Res. 43, D447–D452.
Wood, A.R., Esko, T., Yang, J., Vedantam, S., Pers, T.H., Gustafsson, S., et al., 2014. Defining the role of common variation in the genomic and biological architecture of adult human height. Nat. Genet. 46, 1173–1186.